VISUAL MEASUREMENT METHOD USING A CIRCULAR GROOVE IMAGE FOR MEASURING INTERNAL DEFECTS OF PIPES IN NUCLEAR POWER PLANT

YOUNGSOO CHOI, KYUNGMIN JEONG*, SUNG-UK LEE and SEUNGHO JUNG
Nuclear Robotics Lab. Korea Atomic Energy Research Institute
1045 Daedeokdaero, Yuseong, Daejeon, 305-353, Korea
*Corresponding author. E-mail : kmjeong@kaeri.re.kr

Received November 29, 2007
Accepted for Publication April 5, 2008

During the overhaul period of nuclear power plants in Korea, an ROV(Remotely Operated Vehicle) enters the cold-leg pipes connected with the reactor to examine the state of the thermal sleeves and their positions in the safety injection nozzles. To measure the positions of the thermal sleeves or scratches with video images recorded during the examination, time-varying camera parameters should be known, such as the focal length and principal points used for the capturing each video image. In this paper, we propose a camera calibration and measurement scheme by using a single image containing two circular grooves of a cylindrical nozzle whose radius and distance are known.

KEYWORDS : Absolute Conic, Camera Calibration, Circular Points, Elliptic Contours, Vanishing Points

1. INTRODUCTION

Nuclear power plants provide about 40% of the electric energy consumed in South Korea. In a pressurized water reactor, to cool down the reactor's temperature during shutdown, cooling water is injected into the cold-leg pipes through a safety injection nozzle. Thermal sleeves are mounted inside the safety injection nozzles to reduce the thermal shocks to the weld zone of the safety injection nozzle.

During the overhaul period of the nuclear power plants, in order to examine the state of the thermal sleeves and their attached position, an ROV enters the cold-leg pipes, as shown in Fig. 1. In addition to visual observations, it is necessary to measure the positions of the thermal sleeves and scratches inside the safety injection nozzle from the video images captured during the examination.

In order to measure such features as accurately as possible, the internal camera parameters, such as the focal length and the principal position of the image, should be known as accurate as possible. However, the focal length of the camera varies according to optical zooming operation during the examination, while the principal position of the image can also vary with the frame grabber used for digitizing the image. Thus, a pre-calibration before the examination is ineffective, and table look-up methods which estimate the focal length values with the zoom control inputs have no meaning, because we have no information about the zoom control input values for each video image frame. Thus, it is preferable that the intrinsic parameters of the camera and the capturing device could be calibrated with the video image captured during the examination. In the video image of a safety injection nozzle, we cannot identify sufficiently distinctive points for performing the conventional calibration methods [1,2] based on the known 3-D coordinates for each distinctive point; however, two or more circular grooves around the circumferential direction of the nozzle are observed as elliptic contours, as shown in Fig. 2, and the geometric information of the grooves, such as the radii and the distances between them, can be obtained from the mechanical design drawings.

In this paper, we propose a camera calibration and a measurement method based on the images of two circular grooves whose radii and the distance between them are known. Simulation works were carried to validate the implemented algorithm and its robustness to some noise. Experimental results show that the distance of the concerned point to the reference point could be retrieved with a measuring error in the order of magnitude of 1 mm.

2. PRELIMINARIES

2.1 Camera Model

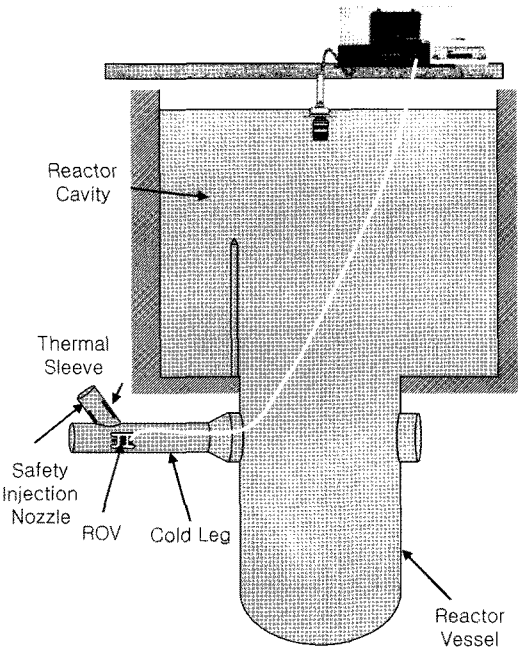

Fig. 1. Diagram of the SI Nozzle Using a ROV.

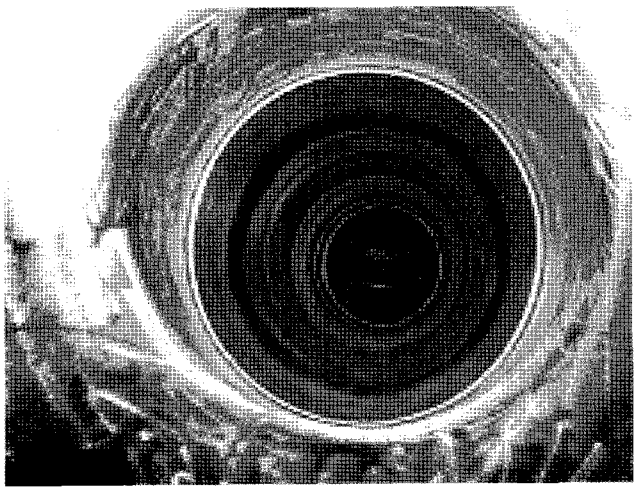

Fig. 2. Captured Video Image of the SI Nozzle.

In this paper, we model the image capturing process with the following pinhole camera model without a lens distortion [4,5,6]:

$$s\begin{bmatrix} x_1 \\ x_2 \\ 1 \end{bmatrix} = \begin{bmatrix} f_1 & 0 & c_1 \\ 0 & f_2 & c_2 \\ 0 & 0 & 1 \end{bmatrix} \begin{bmatrix} r_{11} & r_{12} & r_{13} & t_1 \\ r_{21} & r_{22} & r_{23} & t_2 \\ r_{31} & r_{32} & r_{33} & t_3 \end{bmatrix} \begin{bmatrix} X_1 \\ X_2 \\ X_3 \\ X_4 \end{bmatrix}, \quad (1)$$

$$s\mathbf{x} = \mathbf{K}[\mathbf{R} \mid \mathbf{t}]\tilde{\mathbf{X}} = \mathbf{P}\tilde{\mathbf{X}},$$

$$R = Rot(X_3, R_3)Rot(X_2, R_2)Rot(X_1, R_1)$$

where, $\tilde{\mathbf{X}}=[X_1,X_2,X_3,X_4]^T$ represents a homogeneous coordinate of any 3-D point in the world frame, $x=[x_1,x_2,1]^T$ is the set of image coordinates in a pixel unit for the projected image point of point $\tilde{\mathbf{X}}$, and s is a scale factor for the point.

The matrix **K** is a 3 x 3 internal parameter matrix containing focal parameters, f_1 and f_2, and camera center coordinates, c_1 and c_2. The matrix **R** is a rotation matrix with three rotation angles, R_1, R_2, R_3, while the vector **t** is a translation vector between the world coordinates and the image coordinates.

As depicted in Fig. 3, two circular grooves in a pipe, C_1 and C_2, are projected onto two ellipses, e_1 and e_2, in an image plane. The points O_1 and O_2 are the center points of two circles, and the point O is the focal point of camera. We assume that the radii of the circles are known

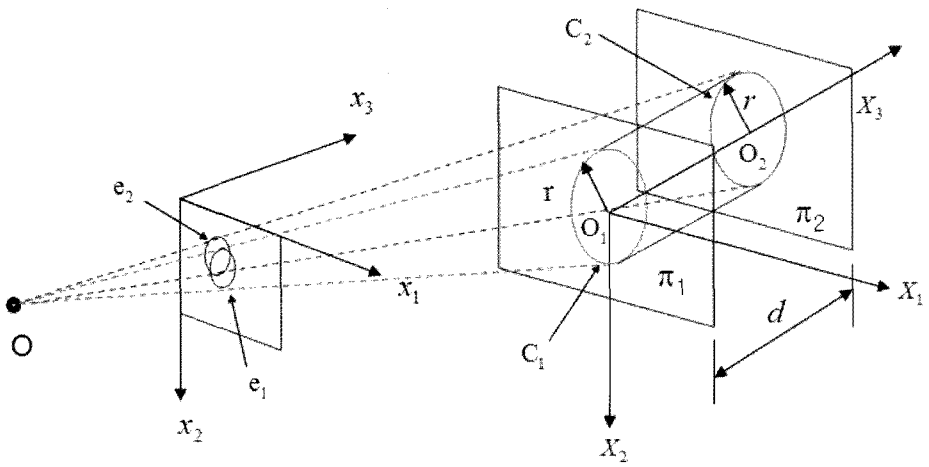

Fig. 3. Image Formation of the Two Circular Grooves

and are the same radius, r. The planes π_1 and π_2, where each circle is located, are parallel to each other, and the distance of the two planes is denoted by d.

The circles C_1 and C_2 can be represented in the homogeneous coordinates, as follows [3].

$$\begin{aligned} C_1 &: X_1^2 + X_2^2 = r^2, X_3 = 0, X_4 = 1 \\ C_2 &: X_1^2 + X_2^2 = r^2, X_3 = d, X_4 = 1 \end{aligned} \quad (2)$$

The circles can also be represented in matrix forms, as follows

$$\begin{aligned} \overline{X}^T \widetilde{C}_1 \overline{X} = 0, X_3 = 0, X_4 = 1 \\ \overline{X}^T \widetilde{C}_2 \overline{X} = 0, X_3 = d, X_4 = 1 \end{aligned} \quad (3)$$

$$\text{where } \widetilde{C}_1 \equiv \begin{bmatrix} 1 & 0 & 0 \\ 0 & 1 & 0 \\ 0 & 0 & -r^2 \end{bmatrix}, \widetilde{C}_2 \equiv \begin{bmatrix} 1 & 0 & 0 \\ 0 & 1 & 0 \\ 0 & 0 & -r^2 \end{bmatrix}, \overline{X} \equiv \begin{bmatrix} X_1 \\ X_2 \\ 1 \end{bmatrix}.$$

If we denote the projection matrices between the image plane and the planes π_1 and π_2 by $\mathbf{P}_1$ and $\mathbf{P}_2$, respectively, then the projected image point X of a point $\overline{X}$ in the circle is represented as follows.

$$s_1 \mathbf{x} = \mathbf{P}_1 \overline{X} = \mathbf{K}\mathbf{Q}_1 \overline{X}, \quad s_2 \mathbf{x} = \mathbf{P}_2 \overline{X} = \mathbf{K}\mathbf{Q}_2 \overline{X}, \quad (4)$$

$$\text{where } \mathbf{Q}_1 \equiv \begin{bmatrix} r_{11} & r_{12} & t_1 \\ r_{21} & r_{22} & t_2 \\ r_{31} & r_{32} & t_3 \end{bmatrix}, \mathbf{Q}_2 \equiv \begin{bmatrix} r_{11} & r_{12} & r_{13}d + t_1 \\ r_{21} & r_{22} & r_{23}d + t_2 \\ r_{31} & r_{32} & r_{33}d + t_3 \end{bmatrix}.$$

Thus, the projected elliptic image e_1 can be represented as the following matrix form by using equation (4).

$$\mathbf{x}^T \widetilde{e}_1 \mathbf{x} = 0, \text{ where } \widetilde{e}_1 \equiv \mathbf{P}_1^{-T} \widetilde{C}_1 \mathbf{P}_1^{-1} = \mathbf{K}^{-T} \mathbf{Q}_1^{-T} \widetilde{C}_1 \mathbf{Q}_1^{-1} \mathbf{K}^{-1} \quad (5)$$

Similarly, the projected elliptic image e_2 can be represented as follows.

$$\mathbf{x}^T \widetilde{e}_2 \mathbf{x} = 0, \text{ where } \widetilde{e}_2 \equiv \mathbf{P}_2^{-T} \widetilde{C}_2 \mathbf{P}_2^{-1} = \mathbf{K}^{-T} \mathbf{Q}_2^{-T} \widetilde{C}_2 \mathbf{Q}_2^{-1} \mathbf{K}^{-1} \quad (6)$$

In order to obtain the internal parameter matrix **K** with the known values $\widetilde{e}_1, \widetilde{e}_2, \widetilde{C}_1, \widetilde{C}_2$, d from the above equations (5) and (6), the rotation matrix **R** and translation vector **t** should be known. However, the rotation matrix **R** and translation vector **t** are also unknown values. Therefore, we used camera calibration approaches utilizing vanishing points, which can extract the internal parameters without considering the rotation and translation parameters [7-13].

2.2 Absolute Conic, Circular Points, Vanishing Points.

From equation (1), any point on the infinite plane, $[X_1, X_2, X_3, 0]^T$ is projected to the image plane by the following equation.

$$s\mathbf{x} = \mathbf{K}[\mathbf{R} \mid \mathbf{t}] \begin{bmatrix} X_1 \\ X_2 \\ X_3 \\ 0 \end{bmatrix} = \mathbf{K}\mathbf{R}\hat{\mathbf{X}} = \mathbf{P}_\infty \hat{\mathbf{X}}, \quad \text{where} \quad \mathbf{P}_\infty \equiv \mathbf{K}\mathbf{R}, \hat{\mathbf{X}} \equiv \begin{bmatrix} X_1 \\ X_2 \\ X_3 \end{bmatrix} \quad (7)$$

The absolute conic Ω consists of the imaginary points satisfying the following equation [4].

$$X_1^2 + X_2^2 + X_3^2 = 0, X_4 = 0. \quad (8)$$

The absolute conic is an ideal conic on the infinite plane with a zero radius and can be represented as the following matrix form.

$$\hat{\mathbf{X}}^T \widetilde{\Omega} \hat{\mathbf{X}} = 0, X_4 = 0, \quad \text{where} \quad \widetilde{\Omega} \equiv \begin{bmatrix} 1 & 0 & 0 \\ 0 & 1 & 0 \\ 0 & 0 & 1 \end{bmatrix} = \mathbf{I}. \quad (9)$$

The image of the absolute conic, ω, consists of the point **x** satisfying the following equation.

$$\mathbf{x}^T \widetilde{\omega} \mathbf{x} = 0, \quad \textit{where} \quad \widetilde{\omega} \equiv \mathbf{P}_\infty^{-T} \widetilde{\Omega} \mathbf{P}_\infty^{-1} = \mathbf{K}^{-T} \mathbf{R}^{-T} \mathbf{I} \mathbf{R}^{-1} \mathbf{K}^{-1} = \mathbf{K}^{-T} \mathbf{K}^{-1}. \quad (10)$$

The symmetric matrix, $\widetilde{\omega}$, representing the image of the absolute conic depends only on the internal parameter matrix, **K**, regardless of the rotation and translation of the camera. Therefore, if we obtain the image of the absolute conic from the scene, we can determine the internal parameter matrix, **K**. However, because the image of the absolute conic is imaginary, we could not find any real point on the conic.

Nonetheless, there are imaginary points on the image of the absolute conic. Circular points Z_1 and Z_2 with respect to the plane normal to the X_3-axis are defined as follows [4].

$$[X_1, X_2, X_3, X_4]^T = [1, \pm i, 0, 0]^T, \quad (11)$$

where i is the imaginary number satisfying $i^2 = -1$.

The circular points of the plane are the intersection points of the plane normal to the X_3-axis and the absolute conic, and they are a complex conjugate pair.

Thus, the projected images z_1 and z_2 of the circular points Z_1 and Z_2 are also located on the image of the absolute conic, ω, as follows:

$$\mathbf{z}_1^T \mathbf{K}^{-T} \mathbf{K}^{-1} \mathbf{z}_1 = 0, \mathbf{z}_2^T \mathbf{K}^{-T} \mathbf{K}^{-1} \mathbf{z}_2 = 0. \quad (12)$$

The vanishing point to the X_3-axis, v_∞, which is the projected image of the point at infinity along the X_3-axis,

$[X_1,X_2,X_3,X_4]^T=[0,0,1,0]^T$ can be represented as follows:

$$\mathbf{v}_\infty = \mathbf{K}[\mathbf{R}\,|\,\mathbf{t}]\begin{bmatrix}0\\0\\1\\0\end{bmatrix} = \mathbf{K}\begin{bmatrix}r_{13}\\r_{23}\\r_{33}\end{bmatrix} \quad (13)$$

The vanishing line l_∞ of plane X_1X_2 is the projected line image of the points on the line at infinity, L_∞, which consists of the points satisfying $X_3 = X_4 = 0$ and any point on the vanishing line, p_∞ can be represented as follows:

$$\mathbf{p}_\infty = \mathbf{K}[\mathbf{R}\,|\,\mathbf{t}]\begin{bmatrix}X_1\\X_2\\0\\0\end{bmatrix} = \mathbf{K}\begin{bmatrix}X_1r_{11}+X_2r_{12}\\X_1r_{21}+X_2r_{22}\\X_1r_{31}+X_2r_{32}\end{bmatrix} \quad (14)$$

Thus, we can show that v_∞ and p_∞ satisfy the following equation from equations (13) and (14).

$$\mathbf{p}_\infty{}^T\mathbf{K}^{-T}\mathbf{K}^{-1}\mathbf{v}_\infty = 0 \quad (15)$$

Because the projected images of the circular points z_1 and z_2 are located on the vanishing line l_∞ of the plane X_1X_2, we can show that the points z_1, z_2, and v_∞ also satisfy the following equations according to equation (15),

$$\mathbf{z}_1{}^T\mathbf{K}^{-T}\mathbf{K}^{-1}\mathbf{v}_\infty = 0, \mathbf{z}_2{}^T\mathbf{K}^{-T}\mathbf{K}^{-1}\mathbf{v}_\infty = 0. \quad (16)$$

Thus, from the identification of the images of the circular points z_1 and z_2 and the vanishing point v_∞ from the scene, we can retrieve four internal parameters, f_1, f_2, c_1, c_2, from equations (12) and (16) and the following equation [13].

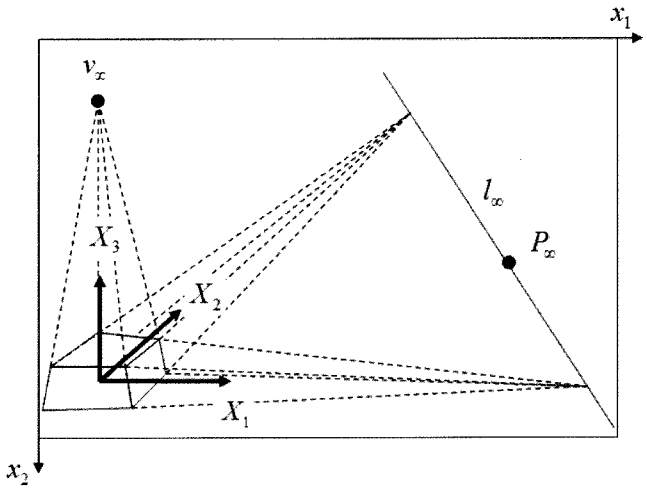

Fig. 4. Vanishing Point and Vanishing Line.

$$\tilde{\omega} = \mathbf{K}^{-T}\mathbf{K}^{-1} = \begin{bmatrix} 1/f_1^2 & 0 & -c_1/f_1^2 \\ 0 & 1/f_2^2 & -c_2/f_2^2 \\ -c_1/f_1^2 & -c_2/f_2^2 & 1+c_1^2/f_1^2+c_2^2/f_2^2 \end{bmatrix} \quad (17)$$

There are many methods for identifying the internal parameters using parallelepiped objects [7-12]. Among the previous works on camera calibration methods using elliptic images [13-15], one method [13] similar to our approach was conducted by using the outside images of cylindrical beverage cans or cups, and most of its results are applicable to our problem. However, in that work, the left and right side outliners connecting the top circle and the bottom circle should be observed in the image in

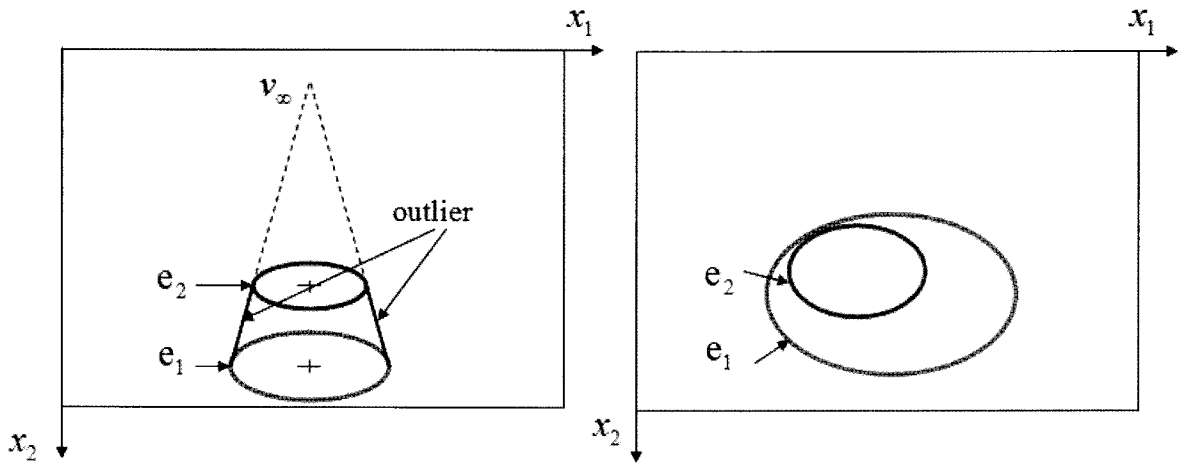

(a) outside image of cylinder (b) inside image of cylinder

Fig. 5. Two Elliptic Images in a Cylinder.

order to identify the vanishing point v_∞, as shown in Fig. 5(a). However, such real images of the outliners could not be observed from the internal view of the cylindrical pipes, as shown in Fig. 5(b).

In the next section, we propose an identification method for the vanishing point from the internal image of a pipe and a camera calibration process using two elliptical images inside a cylinder.

3. PROPOSED CAMERA CALIBRATION STRATEGY

3.1 Identification of Circular Points

The following form represents any circle C on planes normal to the X_3-axis.

$$X_1^2 + X_2^2 + aX_1X_4 + bX_2X_4 + cX_4^2 = 0 \tag{18}$$

We can easily show that such a circle intersects with the line at infinity L_∞ whose X_4 is zero, while the intersection points are only the circulasr points, Z_1 and Z_2. This means that the circles C_1 and C_2 intersect each other at the circular points, Z_1 and Z_2, and the elliptical images of the circles, e_1 and e_2, also intersect at the images of the circular points z_1 and z_2 on the image plane.

Because the circular points Z_1 and Z_2 are a complex conjugate pair, z_1 and z_2 are a complex conjugate pair that could not be observed in real images. In general, because an ellipse has a quadratic form in homogeneous image coordinates, the number of intersection points of the two ellipses is four, and these intersection points are either four real points, two real points and a pair of complex conjugate points, or two pairs of complex conjugate points [16-17].

In the internal images of the cylindrical pipes, the four real intersection points depicted in Fig. 6(a) could not be found. In the case when only complex conjugate intersection points are found, as shown in Fig. 6(b), the points are just the images of the circular points. But when two pairs of a complex conjugate are found as intersection points, as shown in Fig. 6(c) or (d), these two pairs are the images of the circular points corresponding to two planes having two different normal directions, as shown in Fig. 7. Therefore, it is necessary to distinguish which corresponds to the real one among the two pairs of complex conjugated intersection points, and it will be shown in Section 4 that this problem can be solved by using the known radius of the circles.

If we have identified the image of the circular points from the intersection points of two elliptic images, the vanishing line can also be identified, because the images of the circular points are on the vanishing line. Though the images of the circular points are a complex conjugate pair, the vanishing line is a real image.

3.2 Identification of Vanishing Point Along X_3-Axis

Figure 8 shows a cylinder consisting of two circles, C_1 and C_2, and the internal image of that cylinder. Let an arbitrary point on the vanishing line l_∞ be denoted by p_∞.

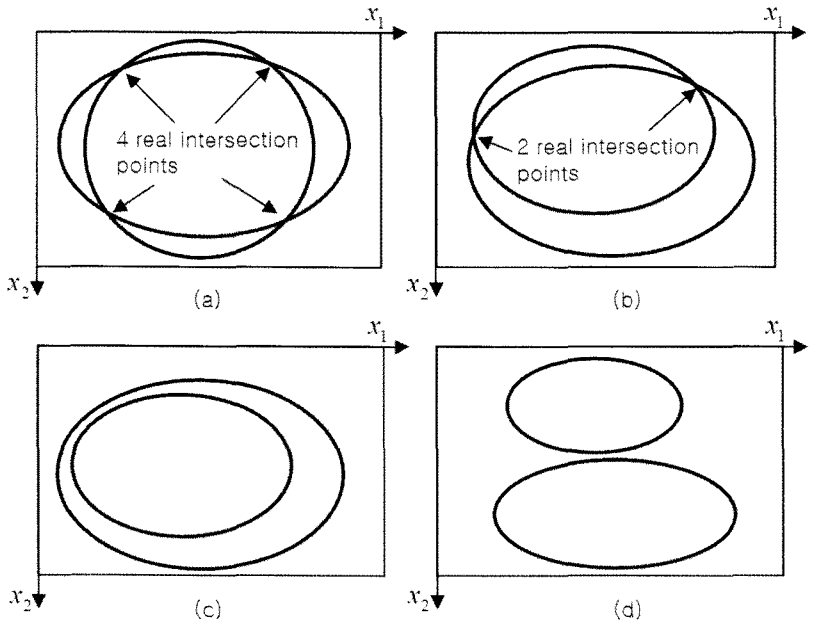

Fig. 6. Intersection Points of Two Ellipses

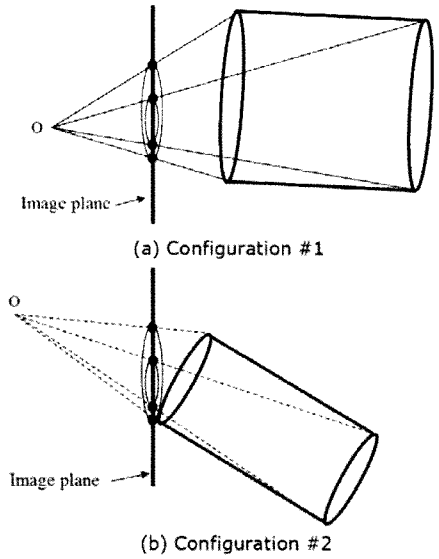

Fig. 7. Two Configurations Projected to the Same Elliptic Images

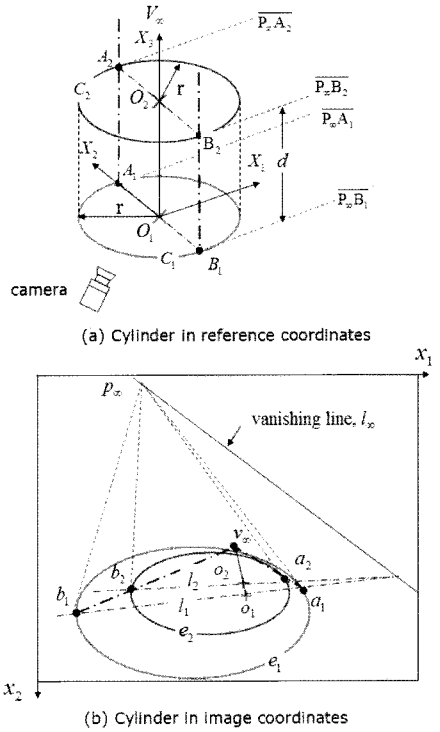

Fig. 8 A Cylindrical Pipe and its Image.

Let $\tilde{e}_1$ and $\tilde{e}_2$ be 3 x 3 matrix representations of the ellipse images e_1 and e_2. With the point p_∞ as a pole, we can obtain the polar line l_1 ($=\tilde{e}_1 p_\infty$) with respect to the ellipse e_1, and the line l_2 ($=\tilde{e}_2 p_\infty$) is also the polar line of the point p_∞ with respect to the ellipse e_2.

Let the points a_1 and b_1 be the intersection points of the ellipse e_1 and the line l_1. In addition, let the points a_2 and b_2 be the intersection points of the ellipse e_2 and the line l_2. The points a_1, b_1, a_2, and b_2 are the image of the points A_1, B_1, A_2, and B_2, respectively. Thus, the polar lines l_1 and l_2 are the images of $\overline{A_1B_1}$ and $\overline{A_2B_2}$ respectively.

Because V_∞, the point at infinity along the X_3-axis, is the intersection point of two outliers, $\overline{A_1A_2}$ and $\overline{B_1B_2}$, the vanishing point, v_∞, can be obtained by computing the intersection point of the lines $\overline{a_1a_2}$ and $\overline{b_1b_2}$.

The images of the center points of the circles, o_1 and o_2, can also be obtained using the pole-polar relationship, as follows [13]:

$$o_1 = \tilde{e}_1^{-1} l_\infty, \quad o_2 = \tilde{e}_2^{-1} l_\infty. \tag{19}$$

3.3 Identification of the External Camera Parameters

As mentioned in Section 2, the internal camera parameters can be retrieved from Eqs. (12) and (16) if the images of the circular points and the vanishing point are identified from the scene. The remaining calibration process for identifying the external camera parameters, such as the rotation and translation from the reference coordinates to the camera coordinates, is similar to other works, and the computation method for the external parameters and radius of the circle can be found in the reference [13].

4. SIMULATIONS AND EXPERIMENTS

4.1 Simulation Results

To verify the calibration algorithm we have proposed, simulation works have been carried out with the artificial images generated from given calibration parameters.

Figure 9 shows generated ellipses, the calculated vanishing points, and the ellipse centers for several cases of varying R_2.

In these cases, 1% random noises are added to the radius of the circles C_1 and C_2 when the ellipse images are generated. Because there are two real intersection points between the two ellipses, we can obtain a unique parameter set, as shown in Table 1.

Because there is no difference in elliptic images while rotating the pipe along the X_3 axis, it is impossible to identify the rotation angle, R_3, about the X_3 axis from the two elliptic images of a cylinder. Thus, the calculated angle R_3 can be quite different from the given value, as shown in Table 1,

Figure 10 shows two cases when there are no real

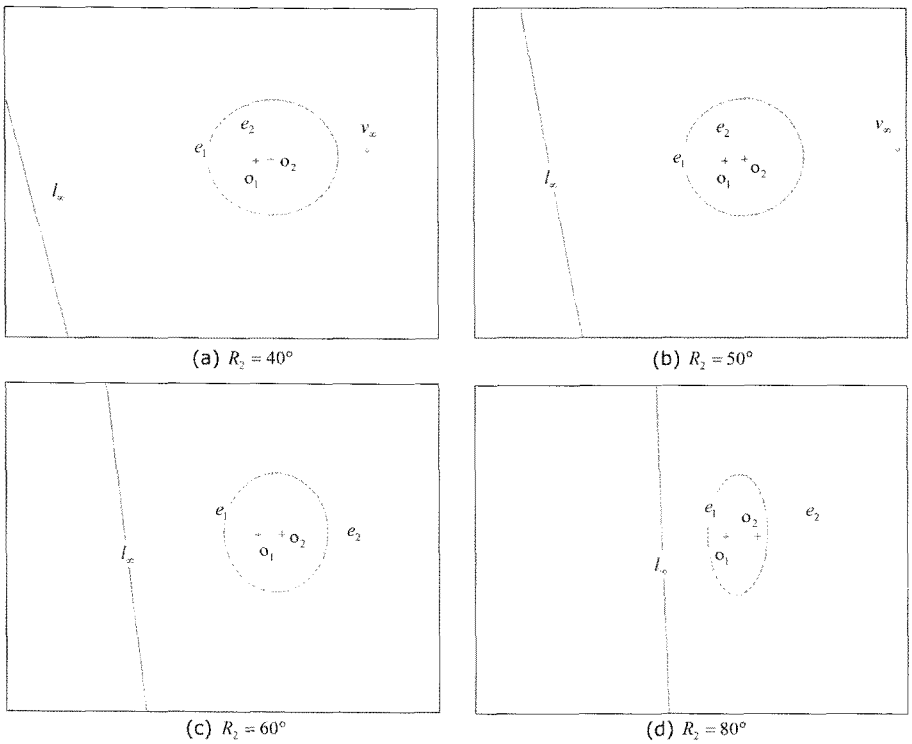

Fig. 9 Vanishing Point and Line at Infinity for Varying R_2 with Real Intersection Points

intersection points between the two ellipses. From two pairs of circular points, we can obtain two sets of parameters, as shown in Table 2.

Two sets of calibrated parameters correspond to two respective pairs of circular points, as mentioned earlier. As shown in Table 2, the radii of circle, r, of the result #1B or the result #2B are similar to the given radius of 200 mm, though the radii of the result #1A and the result #2B are quite different from the real value. Thus, we can easily distinguish which parameter set is the actual one from the comparison of the calculated radius with the real radius.

Table 1. Calculated Parameters for Varying R_2 with Real Intersection Points

	Given Value	R_2(deg)=40°	R_2(deg)=50°	R_2(deg)=60°	R_2(deg)=80°
f_1(mm^{-1})	250.00	249.50	248.85	249.88	250.48
f_2(mm^{-1})	200.00	199.54	199.55	200.58	199.72
c_1(pixel)	320.00	319.47	318.41	318.53	320.29
c_2(pixel)	240.00	240.49	240.25	239.93	240.22
R_1(deg)	10.00	10.25	10.18	9.99	10.05
R_2(deg)	-	40.18	50.32	60.19	79.98
R_3(deg)	5.00	87.69	87.36	86.96	84.59
t_1(mm)	100.00	100.88	102.79	102.86	99.37
t_2(mm)	-50.00	-51.03	-50.40	-49.78	-50.72
t_3(mm)	500.00	498.99	497.06	498.78	500.68
r (mm)	200.00	200.07	199.26	199.07	200.61

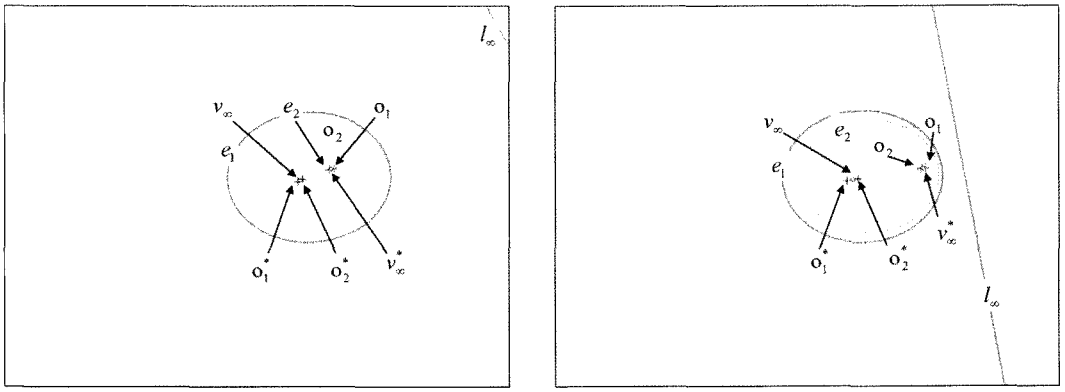

(a) $R_2 = 20°$ (b) $R_2 = 30°$

Fig. 10 Vanishing Point and Line at Infinity for Varying R_2 with No Real Intersection Points

4.2 Experimental Results

We constructed an experimental setup that had several internal circular grooves whose distance between each other and radius were known. The internal radius of the pipe was 298 mm and d, the distance between two reference circular grooves, was 100 mm.

We used a SONY FCB-EX480 color CCD camera with a zoom lens to record the experimental video images with a digital video recorder in AVI motion picture format and converted the images to BMP image files with 640 x 480 resolutions.

The captured images had a little nonlinear lens distortion that is not considered in our image formation model, and we restored the images to the distortion-free images by using the well-known Tsai's calibration algorithm [1].

Figure 11 shows an image of an internal view of the experimental pipe. We computed the calibration parameters and calculated the longitudinal distance from the reference circle, C_1, to several points to validate the proposed method. The real and the estimated longitudinal distances to points P_a, P_b, P_c, and P_d are provided in Table 3.

Figure 12 shows another internal view and Table 4 shows the real and the estimated distances from the reference circle. As shown in Tables 3 and 4, the distance errors were about 3 mm. This result shows that the proposed method is valid because the resultant distance errors were similar to the error corresponding to one pixel, and such accuracy is sufficient to determine the integrity of thermal sleeves and the safety injection nozzle.

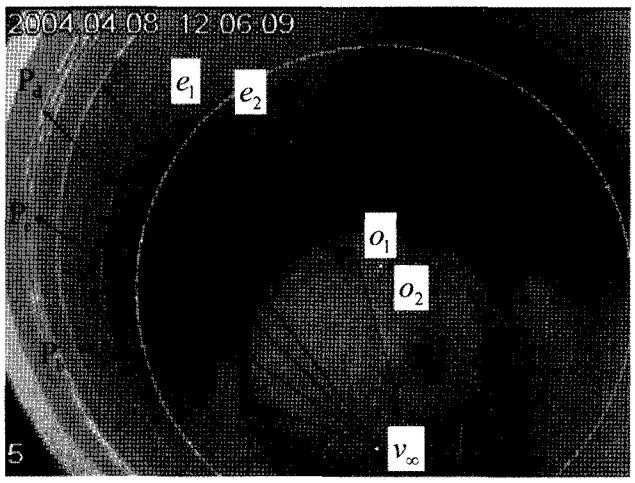

Fig.11. Distance Measurement Experiment #1

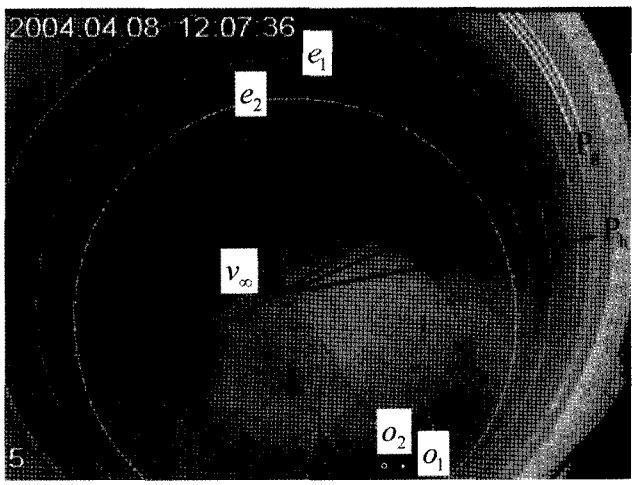

Fig.12. Distance Measurement Experiment #2

Table 2. Calculated Parameters for Varying R_2 with No Real Intersection Points

	Given value	R_2(deg)=20°		R_2(deg)=30°	
		Result #1A	Result #1B	Result #2A	Result #2B
f_1(mm^{-1})	250.00	133.07	251.34	60.82	251.92
f_2(mm^{-1})	200.00	107.14	200.83	54.86	201.00
c_1(pixel)	320.00	437.49	320.71	481.30	321.79
c_2(pixel)	240.00	196.12	240.66	203.11	241.54
R_1(deg)	10.00	-11.90	10.16	-16.08	10.41
R_2(deg)	-	-25.07	19.724	-58.48	29.40
R_3(deg)	5.00	92.00	88.01	94.59	87.92
t_1(mm)	100.00	-86.23	98.85	-143.67	97.26
t_2(mm)	-50.00	35.78	-51.48	12.92	-53.47
t_3(mm)	500.00	522.39	501.09	721.74	502.61
r (mm)	200.00	373.00	199.71	660.99	200.12

Table 3. Longitudinal Distances of Experiment #1

	P_a	P_b	P_c	P_d
Real (mm)	100.0	100.0	140.0	160.0
Calculated (mm)	98.27	98.75	138.52	159.35

Table 4. Longitudinal Distances of Experiment #2

	P_e	P_f	P_g	P_h
Real (mm)	100.0	100.0	200.0	260.0
Calculated (mm)	97.46	100.97	199.68	262.54

5. CONCLUSIONS

In this paper, we have proposed a camera calibration and measurement method using two elliptic contours inside a pipe. It has been shown by simulation and experiments that the proposed method is valid.

The method can be used to measure the positions of the thermal sleeve and scratches from the video images of a safety injection nozzle that are captured by an ROV inside nuclear reactors in Korea. It can also be used to perform visual inspection, defect measurement, and localization of a pipe inspection robot inside pipes.

In further works, we will study a camera calibration method that can also identify a nonlinear lens distortion from a single image.

REFERENCES

[1] R. Y. Tsai, "A Versatile Camera Calibration Technique for High-Accuracy 3D Machine Vision Metrology Using Off-the-Shelf TV Cameras and Lenses," IEEE Journal of Robotics and Automation, Vol. RA-3, No. 4, pp.323-344 (1987).

[2] Z. Zhang," Flexible Camera Calibration By Viewing a Plane From Unknown Orientations," International Conference on Computer Vision, pp. 666-673 (1999).

[3] J. Salvi, X. Armangue, and J. Batlle, "A comparative review of camera calibrating methods with accuracy evaluation," Pattern Recognition 35, pp. 1617-1635 (2002).

[4] R. Hartley and A. Zisserman, Multiple View Geometry in computer vision, Cambridge University Press (2000).

[5] D.A. Forsyth, J. Ponce, Computer Vision A Modern Approach, Prentice Hall (2003).

[6] A. Criminisi, Accurate Visual Metrology from Single and Multiple Uncalibrated Images, Springer (2001).
[7] J.-Y. Guillemaut, A. S. Aguado and J. Illingworth, Using Points at Infinity for Parameter Decoupling in Camera Calibration," Pattern Recognition, Vol.36, No. 5, pp. 1155-1164 (2003).
[8] Jana Kosecka and Wei Zhang,"Video Compass," ECCV, Vol.4, pp.476-490 (2002).
[9] R. Cipolla, T. Drummond and D. Robertson, "Camera calibration from vanishing points in images of architectural scenes," Proc. British Machine Vision Conference, pp.382-391 (1999).
[10] Yong-In, Yoon, Jang-Hwan Im, Dae-Hyun Kim, Jong-Soo Choi , "3D Reconstruction using three vanishing points from a single image," Proc. of International Technical Conference on Circuits/Systems, Computers and Communications (2002).
[11] Marta Wilczkowiak_ Edmond Boyer Peter Sturm, "Camera Calibration and 3D Reconstruction from Single Images Using Parallelepipeds," Proc. of the 8th International Conference on Computer Vision, Vol.1,pp.142-148 (2001).
[12] Guanghui Wanga,b, Hung-Tat Tsuia, Zhanyi Hub, Fuchao Wub,"Camera Calibration and 3D Reconstruction from a Single View Based on Scene Constraints," Image and Vision Computing,Vol. 23,No. 3,pp.311-323 (2005).
[13] Yihong Wu, Guanghui Wang, Fuchao Wu, Zhanyi Hu, "Euclidean Reconstruction of a Circular Truncated Cone only from its Uncalibrated Contours," Image and Vision Computing, Vol.24, No.8 , pp.810-818 (2006)
[14] X. Meng, H. Li and Z. Hu,"A New Easy Camera Calibration Technique Based on Circular Points," Pattern Recognition. Vol. 36, No. 5, pp. 1155-1164 (2003).
[15] Jun-Sik Kim, Ho-Won Kim and In So Kweon, "A camera calibration method using concentric circles for vision applications", The 5th Asian Conference on Computer Vision, pp. 515-520 (2002).
[16] Carlo Colombo alberto Del Bimbo, and Federico Pernici, Metric 3D Reconstruction and Texture Acquisition of Surfaces of Revolution from a Single Uncalibrated View, IEEE Transactions on Pattern Analysis and Machine Intelligence, Vol.27, No.1, pp.99-114 (2005).
[17] Y. H. Wu, X. J. Li, F. C. Wu, and Z. Y. Hu, Coplanar circles, quasi-affine invariance and calibration, *Image and Vision Computing*, Vol.24, No.4, pp:319-326 (2006).